JOURNAL OF MASS SPECTROMETRY, VOL. 32, 351–369 (1997)

SPECIAL FEATURE: TUTORIAL

An Introduction to Quadrupole Ion Trap Mass Spectrometry

Raymond E. March*
Department of Chemistry, Trent University, Peterborough, ON, K9J 7B8, Canada

A concise introduction is presented to the theory and application of quadrupole ion trap mass spectrometry. The presentation of the theoretical treatment is based on a demonstration of the equivalence of the force acting on an ion in a quadrupole field and the force derived from the Mathieu equation; this equivalence permits the application of the solutions of Mathieu's equation to the confinement of gaseous ions. Resonant excitation, collision-induced dissociation, mass spectrometry, tandem mass spectrometry and chemical ionization are discussed in the context of analytical applications. Sample calculations of the trapping parameters q_z and β_z, the axial secular frequency, mass range, mass range extension and the magnitude of the potential well depth are given. © **1997 by John Wiley & Sons, Ltd.**

J. Mass Spectrom. **32**, 351–369 (1997)
No. of Figures: 21 No. of Tables: 0 No. of Refs: 21

KEYWORDS: quadrupole ion trap; mass spectrometry; quadrupole ion trap mass spectrometry; quadrupole mass filter

INTRODUCTION

The quadrupole ion trap is an extraordinary device which functions both as an ion store in which gaseous ions can be confined for a period of time and as a mass spectrometer of considerable mass range and variable mass resolution, all of this and at a pressure of 1 mTorr of helium buffer gas. As a storage device, the ion trap acts as an 'electric field test-tube' for the confinement of gaseous ions, either positively or negatively charged, in the absence of solvent. The confining capacity of the 'electric field test-tube' arises from the formation of a trapping potential well when appropriate potentials are applied to the electrodes of the ion trap. The confinement of gaseous ions in such a test-tube permits the study of gas-phase ion chemistry and the elucidation of ion structures by the use of repeated stages of mass selection known as tandem mass spectrometry. With the advent of new methods by which ions can be formed in the gas phase from polar as well as covalent molecules and introduced subsequently into an ion trap, the range of applications of the quadrupole ion trap is enormous. However, we shall confine ourselves here to the behaviour of the quadrupole ion trap rather than methods of ionization.

In addition to the confinement of ions, the ion trap functions as a mass spectrometer in that the mass/charge ratios of the confined ion species can be measured. The principal method for measuring the mass/charge ratios of confined ions is to tip the potential well, or 'basin,' of the ion trap in a particular 'direction' so that ions tumble out of the potential well and leave the ion trap in order of ascending mass/charge ratio. Alternatively, it can be envisaged that ions are made to leave the basin when one side of the basin is lowered progressively. As each ion species leaves the ion trap in turn, the ions impinge upon an external detector, creating thereby a series of ion signals dispersed in time which constitutes a mass spectrum. Ejection of ions from the potential well is accomplished by ramping in a linear fashion the amplitude of a radiofrequency (r.f.) potential applied to one of the ion trap electrodes; each ion species is ejected from the potential well at a specific r.f. amplitude and, because the initial amplitude and ramping rate are known, the mass/charge ratio can be determined for each ion species upon ejection. This method for measuring mass/charge ratios of confined ions, developed by Stafford *et al.*[1] and known as the 'mass-selective axial instability mode,' made possible the commercialization of the quadrupole ion trap ~14 years ago A prerequisite of this method of mass-selective ion ejection is that ions be herded initially to the centre of the ion trap under the action of momentum-dissipating collisions; helium atoms are used for this purpose.

This relatively simple method of mass-selective operation of the ion trap has led to a revolution in mass spectrometry. It is estimated that more than 4000 ion trap instruments have been sold thus far at a total cost

* Correspondence to: R. E. Marsh.
Contract grant sponsor: Natural Science and Engineering Research Council of Canada.
Contract grant sponsor: Varian Canada.
Contract grant sponsor: Ontario Ministry of Environment and Energy.

CCC 1076–5174/97/040351–19 $17.50

Received 6 February 1997
Accepted 10 February 1997

of about a quarter of a billion US dollars; the diversion of a goodly fraction of this sum from the possible purchase of sector and other instruments has led to considerable reorganization within the mass spectrometry industry. The combination of a quadrupole ion trap interfaced with a gas chromatograph (GC/MS) is now available commercially at a price which permits the acquisition of these instruments by most academic Departments of Chemistry; thus these instruments are now becoming accessible to relatively large numbers of students, both graduate and undergraduate.

The coupling of liquid chromatography (LC) with electrospray (ES) ionization and with mass spectrometry (MS) in the early 1980s, together with the rapid advancement in ion trap technology, have led to the development of new ion trap instruments for the analysis of non-volatile, polar and thermally labile compounds. In 1995, new ion trap instruments (Finnigan's LCQ and GCQ and Bruker-Franzen's ESQUIRE) were introduced, which employ external ion sources with injection of externally generated ions into the ion trap. The major focus for the application of these new instruments, using LC/ESMS, has been the analysis of high molecular weight biopolymers such as proteins, peptides and oligodeoxyribonucleotides. These instruments differ somewhat in electrode size, electrode separation, drive frequency and mass scanning rate from the common GC/MS instruments.

It is hoped that this conversational introduction to quadrupole ion trap spectrometry may give students of all ages an insight into the subtleties and great power of the quadrupole ion trap and an appreciation of the beauty of the basic theory. That the basic theory of operation of quadrupole devices was enunciated almost 100 years before the quadrupole ion trap and the related quadrupole mass filter were invented by Paul and Steinwedel[2] is a shining example of the inherent value of sound basic research. The pioneering work of the inventors was recognized by the award of a 1989 Nobel Prize in Physics to Wolfgang Paul.[3]

In this presentation, references have been given to only those works which may be regarded as landmarks in the field of ion trap mass spectrometry and to those publications which have been used to illustrate specific modes of operation of the ion trap. The reader is directed to detailed accounts by Dawson and Whetten[4] and by Dawson[5] of the early development of quadrupole devices; a full (although a little dated) account of the theory of the ion trap by March *et al.*;[6] reviews by Todd,[7] Cooks *et al.*,[8] Glish and McLuckey[9] and March;[10] and three volumes entitled *Practical Aspects of Ion Trap Mass Spectrometry*[11] which contain accounts from 30 laboratories engaged in ion trap research.

THE POTENTIAL WELL AND THE STRUCTURE OF THE QUADRUPOLE ION TRAP

The trapping potential well created within the electrode assembly of the quadrupole ion trap can be likened to a bowl of parabolic cross-section; ion species are confined in layers in the bowl rather like an exotic drink of several liqueurs arranged carefully and tastefully in horizontal layers according to their density, as shown in Fig. 1(a). Upon tilting the bowl to the right, the layer of least density, corresponding to ions of lowest mass/charge ratio, is poured from the bowl as shown in Fig. 1(b); further tilting of the bowl causes each layer in turn to be poured out. The tilting of the bowl or the lowering of the side of the bowl corresponds to the ramping of the r.f. amplitude; the liqueur glass in Fig. 1(b) corresponds to the detector.

The quadrupole ion trap consists essentially of three rather oddly shaped electrodes which are shown in open array in Fig. 2. Two of the three electrodes are virtually identical and, while having hyperboloidal geometry, resemble small inverted saucers; these saucers are called end-cap electrodes and, in Fig. 2, are distinguishable by the number of holes in the centre of each electrode. One end-cap electrode has a single small central aperture through which electrons and/or ions can be gated periodically and the other has several small apertures arranged centrally also and through which ions pass to a detector; in ion trap instruments with external ion sources, each end-cap electrode has a single perforation. The third electrode is also of hyperboloidal geometry (of two sheets, in this case, rather than one) and is called the ring electrode; it not only resembles a serviette or napkin holder but is of roughly the same size. The ring electrode is positioned symmetrically between two end-cap electrodes as shown in Fig. 3; Fig. 3(a) shows a photograph of an ion trap cut in half along the axis of cylindrical symmetry while Fig. 3(b) is a cross-section of an ideal ion trap showing the asymptotes and the dimensions r_0 and z_0, where r_0 is the radius of the ring electrode in the central horizontal plane and $2z_0$ is the separation of the two end-cap electrodes measured along the axis of the ion trap.

The electrodes in Fig. 3 are truncated for practical purposes, but in theory they extend to infinity and meet the asymptotes shown in the figure. The asymptotes arise from the hyperboloidal geometries of the three electrodes and, in the ideal case, are inclined at an angle of 53° 34′ to the cylindrical axis (viz. the z-axis) of the electrode arrangement. The geometries of the electrodes are defined so as to produce an ideal quadrupole field which, in turn, will produce a parabolic potential well for the confinement of ions (Fig. 1). The potential well is created from the field which exists when an r.f. potential is applied to the ring electrode and the two end-cap electrodes are grounded. However, as shown in Fig. 4, the potential well in the axial direction is of depth $\bar{D}_z$ whereas in the radial direction the depth is $\bar{D}_r$; the value of $\bar{D}_z$ is about twice that of $\bar{D}_r$ so that the potential well resembles more closely a flower vase than a bowl.

For an ideal quadrupole field, the following identity is given (usually with more authority than truth):

$$r_0^2 = 2z_0^2 \quad (1)$$

so that once the magnitude of r_0 is given the sizes of all three electrodes and the electrode spacings are fixed. However, it has been pointed out by Knight[12] that, contrary to Eqn. (1), the ratio of z_0^2 to r_0^2 is not necessarily restricted to 2. Regardless of the value of this ratio, the size of the ion trap is determined largely by

the magnitude of r_0 and, in the majority of commercial ion traps in use today r_0 is either 1.00 or 0.707 cm.

THE SUCCESSFUL SEARCH FOR A THEORY OF ION TRAP OPERATION

The motions of ions in quadrupole devices differ greatly from the straight lines and arcing curves of ions in field-free regions and in magnetic and electrostatic sectors, respectively. The quadrupole ion trap and the quadrupole mass filter or analyser are described as *dynamic* instruments since ion trajectories in these instruments are influenced by a set of time-dependent forces (which render the trajectories mathematically somewhat more difficult to predict compared with sector instruments). Sector instruments are described as *static* devices in that the field is maintained at a constant value for transmission of an ion. In *quadrupole* instruments, a quadrupole field is established when a potential is applied to electrodes that have a hyperbolic geometric form. We must now search for a theory of ion motion which accounts for the movement of charged particles in a quadrupole field but, first, let us consider the forces acting on a single ion within a quadrupole field.

An ion in a quadrupole field

An ion in a quadrupole field experiences strong focusing in that the restoring force, which drives the ion back towards the centre of the device, increases as the ion deviates from the centre of the device. The search for a theory of ion motion is not a long one since it has been found that the motion of ions in a quadrupole field can be described mathematically by the solutions to the second-order linear differential equation described originally by Mathieu;[13] this equation is known as the Mathieu equation. From Mathieu's investigation of the mathematics of vibrating stretched skins, he was able to describe solutions in terms of regions of stability and instability. We can apply these solutions and the ideas of stability and instability to describe the trajectories of ions confined in quadrupole devices and to define the limits to trajectory stability. In order to adopt the solutions to the Mathieu equation, we must verify that the equation of motion of an ion confined in a quadrupole device can be described by the Mathieu equation. The path that we shall follow is one wherein we obtain an expression for a force (mass × acceleration) in mathieu's equation, and compare that expression with one for the force on an ion in a quadrupole field. This comparison, which is laid out below in simple mathematical terms, allows us to express the magnitudes and frequencies of the potentials applied to ion trap electrodes, the size of the ion trap and the mass/charge ratio of ions confined therein in terms of Mathieu's dimensionless parameters, a_u and q_u. On this basis, we shall adopt the idea of stability regions in a_u, q_u space in order to discuss the confinement, and limits thereto, of gaseous ions in quadrupole devices.

The Mathieu equation

The canonical or commonly accepted form of the Mathieu equation is

$$\frac{d^2u}{d\xi^2} + (a_u - 2q_u\cos 2\xi)u = 0 \tag{2}$$

where u represents the coordinate axes x, y and z, ξ is a dimensionless parameter equal to $\Omega t/2$ such that Ω must be a frequency as t is time, and a_u and q_u are additional dimensionless parameters known as trapping parameters. The introduction of Ω here is not entirely serendipitous since it will reappear as the radial frequency (in rad s^{-1}) of the r.f. potential applied to the ring electrode. Now it can be shown by substituting $\xi = \Omega t/2$ (from Eqn (2)) that

$$\frac{d^2u}{dt^2} = \frac{\Omega^2}{4}\frac{d^2u}{d\xi^2} \tag{3}$$

Substitution of Eqn (3) into Eqn (2), multiplying throughout by m and rearranging yields

$$m\frac{d^2u}{dt^2} = \frac{-m\Omega^2}{4}(a_u - 2q_u\cos\Omega t)u \tag{4}$$

We note that the left-hand side of Eqn (4) can represent the force on an ion, that is, mass times acceleration in each of the x, y and z directions.

Now the field in quadrupole devices is uncoupled so that the forces in the three coordinate directions may be determined separately. Let us then consider the force in the x-direction, F_x, experienced by an ion of mass m and charge e at any point within a quadrupole field:

$$F_x = ma = m\frac{d^2x}{dt^2} = -e\frac{\partial\phi}{\partial x} \tag{5}$$

where a is the acceleration of the ion, e is the electronic charge and ϕ is the potential at any point (x, y, z) within the field. Similar expressions for F_y and F_z can be obtained. It should be noted that Eqn (5) relates the force on an ion to the field within the ion trap. The quadrupole potential ϕ can be expressed as

$$\phi = \frac{\phi_0}{r_0^2}(\lambda x^2 + \sigma y^2 + \gamma z^2) \tag{6}$$

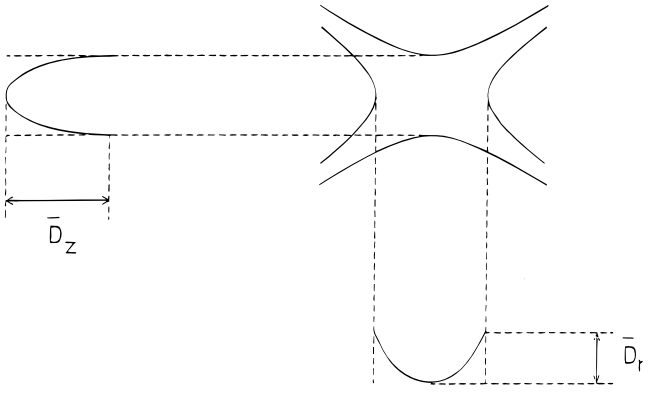

Figure 4. Representation of the parabolic trapping potential wells of depths $\bar{D}_z$ and $\bar{D}_r$.

where ϕ_0 is the applied electric potential (which we shall see later is an r.f. potential either alone or in combination with a direct current (d.c.) potential), λ, σ and γ are weighting constants for the x, y and z coordinates, respectively, and r_0 is a constant which is defined separately depending on whether the quadrupole device is an ion trap or mass filter. It can be seen from Eqn (6) that the potential increases quadratically with x, y and z. In any electric field, it is essential that the Laplace condition, which requires that the second differential of the potential at a point be equal to zero, be satisfied; the Laplace condition ensures that the field in the x, y and z directions is linear. When that is done, it is found that

$$\lambda + \sigma + \gamma = 0 \tag{7}$$

For the ion trap, $\lambda = \sigma = 1$ and $\gamma = -2$, whereas for the quadrupole mass filter $\lambda = -\sigma = 1$ and $\gamma = 0$. Substituting the values $\lambda = \sigma = 1$ and $\gamma = -2$ into Eqn (6), we obtain the following expression for the potential at any point within the quadrupole field in a quadrupole ion trap:

$$\phi_{x,y,z} = \frac{\phi_0}{{r_0}^2}(x^2 + y^2 - 2z^2) \tag{8}$$

This equation can be transformed into cylindrical coordinates by employing the standard transformations $x = r\cos\theta$, $y = r\sin\theta$, $z = z$. Thus, Eqn (8) becomes

$$\phi_{r,z} = \frac{\phi_0}{{r_0}^2}(r^2\cos^2\theta + r^2\sin^2\theta - 2z^2) \tag{9}$$

When we apply the trigonometric identity $\cos^2 + \sin^2 = 1$, we obtain

$$\phi_{r,z} = \frac{\phi_0}{{r_0}^2}(r^2 - 2z^2) \tag{10}$$

The applied electric potential, ϕ_0 (that is, applied to the ring electrode), is either an r.f. potential $V\cos\Omega t$ or a combination of a d.c. potential, U, of the form

$$\phi_0 = U + V\cos\Omega t \tag{11}$$

where Ω is the angular frequency (in rad s^{-1}) of the r.f. field. Note that Ω is equal to $2\pi f$, where f is the frequency in hertz.

When the expression for ϕ_0 as given by Eqn (11) and $\lambda = 1$ are substituted into Eqn (6) and ϕ is differentiated with respect to x, one obtains the following expression for the potential gradient:

$$\frac{\partial\phi}{\partial x} = \frac{2x}{{r_0}^2}(U + V\cos\Omega t) \tag{12}$$

Substitution of Eqn (12) into Eqn (5) yields an expression for the force on an ion:

$$m\frac{d^2x}{dt^2} = \frac{-2e}{{r_0}^2}(U + V\cos\Omega t)x \tag{13}$$

We can now compare directly the terms on the right-hand sides of Eqns (4) and (13), recalling that u represents x, to obtain

$$a_x = \frac{8eU}{m{r_0}^2\Omega^2}; \qquad q_x = \frac{-4eV}{m{r_0}^2\Omega^2} \tag{14}$$

When this derivation is repeated to obtain the force on an ion in the y-direction in a quadrupole mass filter, one finds that $q_x = -q_y$; this relationship is obtained since $\lambda = \sigma = -1$. For the quadrupole ion trap, it is found that $q_x = q_y$; this equality is found since $\lambda = \sigma = 1$. It is suggested that it would be instructive for the reader to derive similarly the a_z and q_z trapping parameters (Eqn (15)) which are used frequently in discussions of the stability diagram of the quadrupole ion trap; in this case, $\lambda = \sigma = 1$ and $\gamma = -2$.

$$a_z = \frac{-8eU}{m{r_0}^2\Omega^2}; \qquad q_z = \frac{4eV}{m{r_0}^2\Omega^2} \tag{15}$$

Let us ignore a_z (which is proportional to U, a d.c. potential) for the present since most commercial ion trap instruments do not offer the flexibility of applying a d.c. potential to the electrodes; thus a_z is equal to zero such that the most common mode of ion trap operation is said to correspond to operation on the q_z axis. The expression for q_z in Eqn (15) contains the mass/charge ratio for a given ion, the size of the ion trap, r_0, the amplitude V of the r.f. potential and the radial frequency Ω, that is, all of the parameters which we shall need in order to understand the various operations of the ion trap. The solutions to the Mathieu equation are now accessible to us and can be interpreted in terms of trajectory stability (and instability) in each of the x, y (or r) and z directions, of confinement when conditions correspond simultaneously to trajectory stability in more than one direction and of trajectory characteristics such as the fundamental secular frequencies of ion motion in the radial, r, and axial, z, directions.

The potentials on the electrodes

We can now verify the potentials on the ring and end-cap electrodes in the following manner with reference to Fig. 4 and Eqn (10). Consider the intersection of the central radial plane with the surface of the ring electrode, such that $z = 0$ and $r = r_0$; the potential at the ring electrode is given by

$$\phi_{r_0,0} = \frac{\phi_0}{{r_0}^2}{r_0}^2 = \phi_0 \tag{16}$$

Now consider the intersection of the central axis of cylindrical symmetry with the surface of either end-cap electrode, such that $r = 0$ and $z = z_0$; recalling the identity of Eqn (1) and the potential of Eqn (10), the potential at each end-cap electrode is given by

$$\phi_{0,z_0} = \frac{\phi}{{r_0}^2}(-2{z_0}^2) = -\phi \tag{17}$$

However, no commercial quadrupole ion trap is operated in this fashion; rather, the end-cap electrodes are held at ground potential (except for the imposition of oscillating potentials of low amplitude, hundreds of millivolts to a few volts). The net effect of applying ϕ to the ring electrode and grounding the end-cap electrodes is to half the mass range of the ion trap as a mass spectrometer.

In order to verify the potentials on the ring and end-cap electrodes in the commercial ion trap, an alter-

native electrode equation to Eqn (10) must be used; this equation is

$$\phi_{r,z} = \frac{\phi_0(r^2 - 2z^2)}{2r_0^2} + c \quad (18)$$

where c is a constant. The ring electrode potential (Eqn (18) with $z = 0$, $r = r_0$) is given by

$$\phi_{r_0,0} = \frac{\phi_0 r_0^2}{2r_0^2} + c = \phi_0 \quad (19)$$

from which we obtain $c = \phi_0/2$. The potential at the end-cap electrodes ($r = 0$ and $z = z_0$) is given by

$$\phi_{0,z_0} = \frac{-2\phi_0 z_0^2}{2r_0^2} + \frac{\phi_0}{2} = 0 \quad (20)$$

Hence Eqn (18) reduces to

$$\phi_{r,z} = \frac{\phi_0(r^2 - 2z^2)}{2r_0^2} + \frac{\phi_0}{2} \quad (21)$$

The constant term does not change the equations of motion derived from the partial differentials, but the potential along the asymptotes of the hyperbolas is changed. It should be noted that an ion at the centre of a commercial ion trap experiences a potential of $\phi_0/2$ but no net field and 'sees' a potential of $-\phi_0/2$ on the end-cap electrodes and a potential of $\phi_0/2$ on the ring electrode.

The 'stretched' ion trap

As we discussed above, the electrodes of the ion trap are truncated in order to obtain a practical working instrument but this truncation introduces higher-order multipole components to the potential:

$$\phi_{r,z} = C_0^0 + C_1^0 z + C_2^0(\tfrac{1}{2}r^2 - z^2) + C_3^0 z(\tfrac{3}{2}r^2 - z^2) + C_4^0(\tfrac{3}{8}r^4 - 3r^2z^2 + z^4) + \cdots \quad (22)$$

The C_n^0 coefficients, were $n = 0$, 1, 2, 3 and 4, correspond to monopole, dipole, quadrupole, hexapole and octopole components, respectively, of the potential $\phi_{r,z}$. For the pure quadrupole ion trap, only the coefficients corresponding to $n = 0$ and $n = 2$ are non-zero.

In order to compensate for these higher order multipole components, the electrodes of most commercial devices prior to 1995 are assembled in such a way that the distance between the end-cap electrodes has been increased or 'stretched;' the value of z_0 has been increased by 10.6%. However, there was no corresponding modification of the shapes of the electrodes, which would be required in order to maintain a purely quadrupolar geometry.

The immediate consequences are that the asymptotes to the end-cap electrodes no longer coincide with those for the ring electrode. Furthermore, $r_0^2 \neq 2z_0^2$. In order to compensate, in part, for the stretching of the ion trap, the trapping parameters are now calculated using the actual values of z_0 and r_0, as follows:

$$a_r = \frac{8eU}{m(r_0^2 + 2z_0^2)\Omega^2}; \qquad q_r = \frac{-4eV}{m(r_0^2 + 2z_0^2)\Omega^2} \quad (23)$$

and

$$a_z = \frac{-16eU}{m(r_0^2 + 2z_0^2)\Omega^2}; \qquad q_z = \frac{8eV}{m(r_0^2 + 2z_0^2)\Omega^2} \quad (24)$$

When $r_0^2 = 2z_0^2$ is substituted into Eqn (24), we obtain the trapping parameters given in Eqn (15). It should be noted that for the ion trap in the LCQ and GCQ instruments, $r_0 = 0.707$ cm and $z_0 = 0.785$ cm such that the geometry has been stretched by $\sim 57\%$.

REGIONS OF ION TRAJECTORY STABILITY

Quadrupole ion trap operation is concerned with the criteria that govern the stability (and instability) of the trajectory of an ion within the field, that is, the experimental conditions that determine whether an ion is stored within the device or is ejected from the device and either lost or detected externally.

The solutions to Mathieu's equation are of two types: (i) periodic but unstable and (ii) periodic and stable. Solutions of type (i) are called Mathieu functions of integral order and form the boundaries of unstable regions on the stability diagram. The boundaries, which are referred to as *characteristic curves* or *characteristic values*, correspond to those values of a new trapping parameter, β_z, which are integers, that is, 0, 1, 2, 3, ...; β_z is a complex function of a_z and q_z to which we shall return. The boundaries represent, in practical terms, the point at which the trajectory of an ion becomes unbounded.

Solutions of type (ii) determine the motion of ions in an ion trap. The stability regions corresponding to stable solutions of the Mathieu equation in the z-direction are shaded and labelled z-stable in Fig. 5(a). The stability regions corresponding to stable solutions

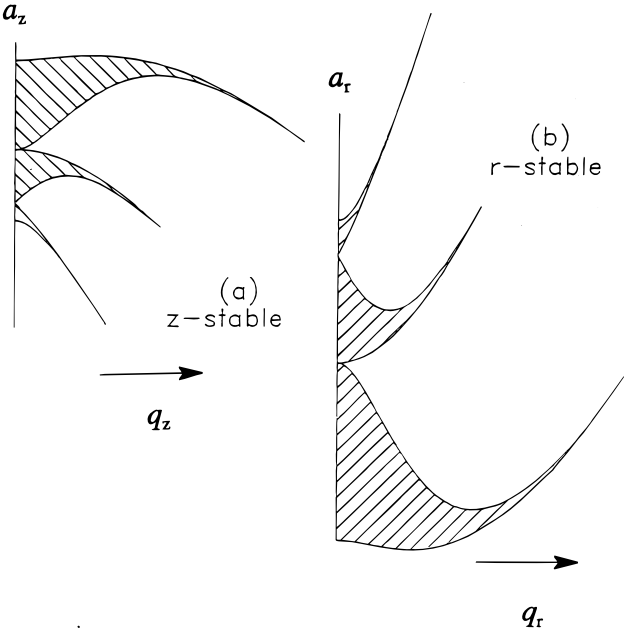

Figure 5. Several Mathieu stability regions for the three-dimensional quadrupole field. (a) Diagrams for the z-direction of (a_z, q_z) space; (b) diagrams for the r-direction of (a_z, q_z) space.

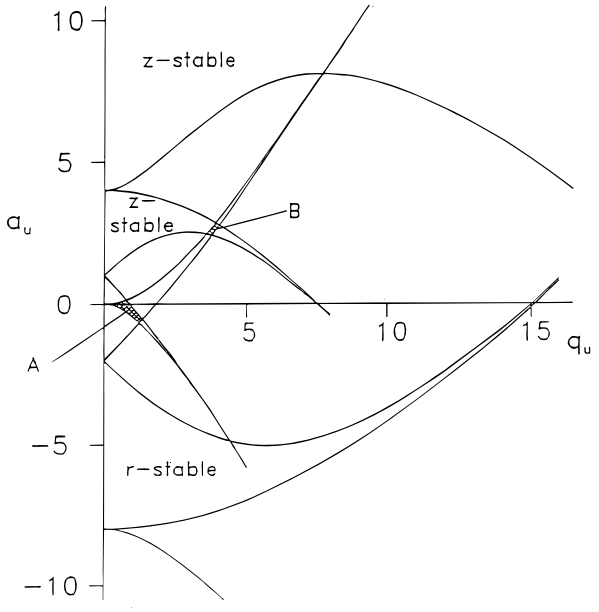

Figure 6. Mathieu stability diagram in (a_z, q_z) space for the quadrupole ion trap in both the r- and z-directions. Regions of simultaneous overlap are labelled A and B.

of the Mathieu equation in the r-direction are shaded and labelled r-stable in Fig. 5(b); it can be seen that they are doubled in magnitude along the ordinate and inverted. It is seen from Eqns (23) and (24) that $a_z = -2a_r$ and $q_z = -2q_r$, that is, the stability parameters for the r- and z-directions differ by a factor of -2.

Ions can be stored in the ion trap provided that their trajectories are stable in the r- and z-directions simultaneously; such trajectory stability is obtained in the region closest to the origin, that is, region A in Fig. 6, which is plotted in a_u, q_u space, that is, where a_u is plotted against q_u. Regions A and B are referred to as stability regions; region A is of the greatest importance at this time (region B remains to be explored) and is shown in greater detail in Fig. 7. The coordinates of the stability region in Fig. 7 are the Mathieu parameters a_z and q_z. Here, we plot a_z versus q_z rather than a_u versus q_u, which is unnecessarily confusing because $u = r, z$. In Fig. 7, the $\beta_z = 1$ stability boundary intersects with the q_z axis at $q_z = 0.908$; this working point is that of the ion of lowest mass/charge ratio (that is, low-mass cut-off, as discussed below) which can be stored in the ion trap.

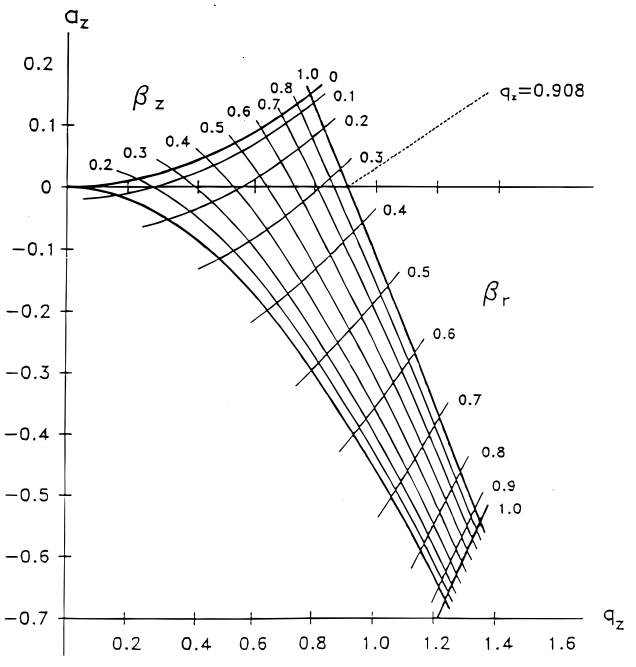

Figure 7. Stability diagram in (a_z, q_z) space for the region of simultaneous stability in both the r- and z-directions near the origin for the three-dimensional quadrupole ion trap; the iso-β_r and iso-β_z lines are shown in the diagram. The q_z-axis intersects the $\beta_z = 1$ boundary at $q_z = 0.908$, which corresponds to q_{max} in the mass-selective instability mode.

SECULAR FREQUENCIES

A three-dimensional representation of an ion trajectory in the ion trap, as shown in Fig. 8, has the general appearance of a Lissajous curve or figure-of-eight composed of two fundamental frequency components, $\omega_{r,0}$ and $\omega_{z,0}$ of the secular motion.[14] The description of 'fundamental' infers that there exist other higher order (n) frequencies and the entire family of frequencies is described by $\omega_{r,n}$ and $\omega_{z,n}$. These secular frequencies are given by

$$\omega_{u,n} = (n + \tfrac{1}{2}\beta_u)\Omega, \qquad 0 \leqslant n < \infty \tag{25}$$

and

$$\omega_{u,n} = -(n + \tfrac{1}{2}\beta_u)\Omega, \qquad -\infty < n < 0 \tag{26}$$

where

$$\beta_u \approx \sqrt{\left(a_u + \frac{{q_u}^2}{2}\right)} \tag{27}$$

for $q_r < 0.2$ and $q_z < 0.4$. It should be noted that while the fundamental axial secular frequency, $\omega_{z,0}$, is usually

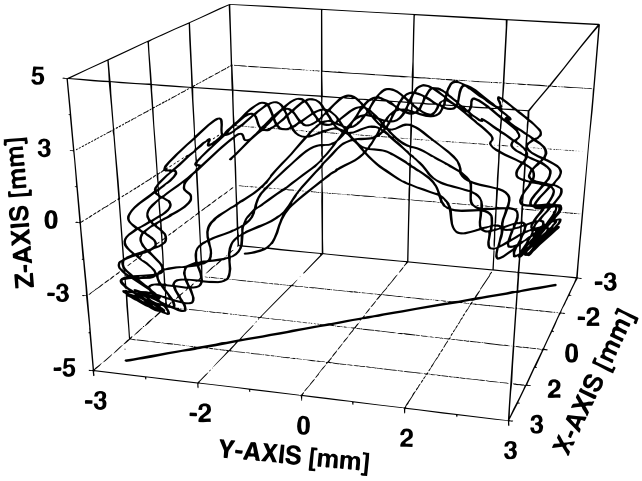

Figure 8. Trajectory of a trapped ion of m/z 105. The initial position was selected randomly from a population with an initial gaussian distribution (FWHM of 1 mm); $q_z = 0.3$; zero initial velocity. The projection on to the x–y plane illustrates planar motion in three-dimensional space. The trajectory develops a shape which resembles a flattened boomerang. Taken from Ref. 14.

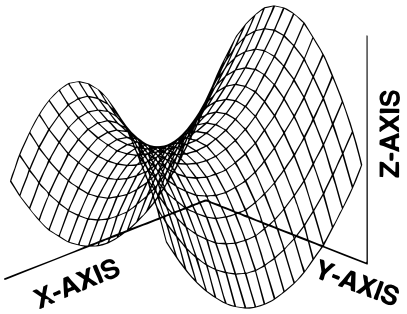

Figure 9. Pure quadrupole field, or potential surface, for a quadrupole ion trap. Note the four poles of the surface and the similarity of the field shape to the trajectory in Fig. 8.

given in units of hertz in the literature and referred to simply as ω_z, it should be given in rad s^{-1}. At this time, the higher order frequencies are of little practical significance.

It should be noted further that the definition of β_z given in Eqn (27) is only an approximation, known as the Dehmelt approximation after Hans Dehmelt, who shared the 1989 Nobel Prize in Physics along with Norman Ramsey and Wolfgang Paul; β_u is defined precisely by a continued fraction expression in terms of a_u and q_u:

$$\beta_u^2 = a_u + \cfrac{q_u^2}{(\beta_u+2)^2 - a_u - \cfrac{q_u^2}{(\beta_u+4)^4 - a_u - \cfrac{q_u^2}{(\beta_u+6)^2 - a_u - \cdots}}} + \cfrac{q_u^2}{(\beta_u-2)^2 - a_u - \cfrac{q_u^2}{(\beta_u-4)^2 - a_u - \cfrac{q_u^2}{(\beta_u-6)^2 - a_u - \cdots}}} \quad (28)$$

The resemblance of the simulated ion trajectory shown in Fig. 8 to a roller-coaster ride is due to the motion of an ion on the potential surface shown in Fig. 9. The oscillatory motion of the ion results from the undulations of the potential surface which can be envisaged as rotation of the potential surface. The simulation of the ion trajectory was carried out using the ITSIM simulation program,[15] while the potential surface was generated[16] from Eqn (22) by calculating $\phi_{r,z}$ for $C_2^0 = 1$ and all of the other coefficients equal to zero for increment steps of 1 mm in both the radial and axial directions.

RESONANT EXCITATION

As the motion of ions confined in a quadrupole ion trap is characterized by two secular frequencies, axial and radial, ion motion can be excited upon resonant irradiation at either or both of these frequencies. Such irradiation can be effected by applying a small supplementary oscillating potential of a few hundred millivolts across the end-cap electrodes, that is, in dipolar mode. Resonant excitation, using the axial secular frequencies of confined ions, has become a powerful technique in quadrupole ion trap mass spectrometry owing to the utilization of predetermined waveforms composed of specified frequencies or frequency ranges. Prior to resonant excitation of ion trajectories, ions are focused collisionally to the vicinity of the centre of the ion trap under the influence of collisions with helium buffer gas atoms. This process is described as 'ion cooling' in that ion kinetic energies are reduced to $\sim$0.1 eV, corresponding to $\sim$800 K as calculated from $3RT/2 = 0.1$ eV. Ion excursions from the centre of the ion trap are less than 1 mm.

Resonant excitation of cooled ions, under the influence of a supplementary potential oscillating at the axial secular frequency of a specific ion species and with an amplitude of only a few hundred millivolts, causes those ions to move away from the ion trap centre such that they experience a greater trapping field. This process of ion excitation is often referred to as 'tickling.' The ions are accelerated further by the trapping field such that they can achieve kinetic energies of tens of electronvolts.

Resonant excitation is used in the following ways. (i) To remove unwanted ions during ionization so as to isolate a narrow range of mass/charge ratios; in this case, wavebands of frequencies are applied to the end-cap electrodes to excite and eject many ion species simultaneously leaving a single ion species (or a small range of mass/charge ratios) isolated within the ion trap. (ii) To increase ion kinetic energy so as to promote endothermic ion–molecule reactions. (iii) To increase ion kinetic energy so as to deposit internal energy in ions through momentum-exchange collisions with helium atoms; in the limit, ions dissociate. This mode of resonant excitation is discussed in more detail under collision-induced dissociation. (iv) To increase kinetic energy so as to move ions close to an end-cap electrode where an image current can be detected. This mode permits the non-destructive measurement and re-measurement of the mass/charge ratio of confined ions. (v) To increase kinetic energy so as to cause ions to escape from the trapping potential and be ejected. This mode can be used either to eject unwanted ions, as in ion isolation, or to eject ions mass selectively while the applied frequency is swept. (vi) To eject ions while the amplitude V of the main r.f. potential is being ramped up. This mode, known as axial modulation, is used in conjunction with an r.f. ramp so that ions come into resonance with a fixed frequency of $\sim 6\ V_{(p-p)}$ just before their trajectories are made unstable. In this case, ions of low mass/charge ratio are removed from the perturbing influences of ions of higher mass/charge ratio and are detected with enhanced resolution. In axial modulation, the resonant frequency is just less than half the main drive frequency Ω. Resonant excitation at lower frequencies has been used with great success to extend the normal mass range of the ion trap.

CALCULATIONS

On many occasions while working with a quadrupole ion trap, it becomes necessary to calculate some of the ion trapping parameters such as q_z, low-mass cut-off

value (LMCO, see below), β_z, the secular frequency ω_z and the potential well depth $\bar{D}_z$. In modern ion trap instruments, these calculations can be carried out using the accompanying software, but it is instructive to examine the manner in which each of the following parameters is calculated.

Let us consider an ion of butylbenzene (m/z 134) in a normal stretched ion trap which has a ring electrode of radius $r_0 = 1.00$ cm and with $z_0 = 0.783$ cm (corresponding to an electrode spacing, $2z_0$, of 15.66 mm) and under the following conditions:

$$U = 0; \quad V = 757 \text{ V}_{(0-\text{p})} \text{ at } 1.05 \text{ MHz}$$

$$\Omega = 2\pi f = 2\pi \times 1.05 \times 10^6 \text{ rad s}^{-1}$$

$$m = \frac{134 \text{ Da}}{\text{Avogadro's number}} = \frac{134 \times 10^{-3} \text{ kg mol}^{-1}}{6.022 \times 10^{23} \text{ mol}^{-1}}$$

(a) q_z and LMCO

From Eqn (24), we recall that

$$q_z = \frac{8\,eV}{m(r_0^2 + 2z_0^2)\Omega^2}$$

Thus,

$$q_z = \frac{8(1.602 \times 10^{-19} \text{ C}) \times (757 \text{ kg m}^2 \text{ s}^{-2} \text{ C}^{-1})(6.022 \times 10^{23} \text{ mol}^{-1})}{(134 \times 10^{-3} \text{ kg mol}^{-1})[(1.000 + 1.226)10^{-4} \text{ m}^2] \times (2\pi \times 1.05 \times 10^6 \text{ s}^{-1})^2}$$

$$= 0.450$$

We have now calculated that m/z 134 has a q_z value of 0.450 under these conditions, but what is the LMCO value at q_z slightly less than 0.908? Since $m \times q_z =$ constant at constant V from Eqn (24), the LMCO value can be calculated as

$$\text{LCMO} \times 0.908 = m/z\ 134 \times 0.450$$

Rearranging,

$$\text{LCMO} = (m/z\ 134 \times 0.450)/0.908$$

$$= m/z\ 66.4$$

That is, with a potential of 757 $V_{(0-p)}$ applied to the ring electrode, only those ions of $m/z > 66.4$ will be stored. The potential V to be applied to the ring electrode to effect a given LCMO is given as

$$V = [\text{LCMO} \times 757 \text{ V}_{(0-\text{p})}]/m/z\ 66.4$$

$$= (11.40 \times \text{LCMO})\text{V}_{(0-\text{p})}.$$

This calculation is particularly useful when an ion is to be fragmented and one wishes to know the low mass/charge limit for fragment ions stored, that is, the low-mass cut-off.

(b) β_z

From Eqn (27), we see that β_z is given approximately by $\sqrt{(q_z^2/2)}$, hence when $q_z = 0.450$, $\beta_z = 0.318$. However, we have exceeded the limit of the approximation relating q_z and β_z and so the calculated value of β_z is high by about 5%. For m/z 1340, where $q_z = 0.0450$ such that the above approximation is valid, the value of $\beta_z = 0.0318$.

(c) ω_z

From Eqn (25), the fundamental axial secular frequency, ω_z (or, more properly, $\omega_{z,0}$), is given by $\beta_z\Omega/2$. Thus, when $\beta_z = 0.318$ and $\Omega = 2\pi \times 1.05 \times 10^6$ rad s^{-1}, $\omega_z = 1.049 \times 10^6$ rad s^{-1} or, more conventionally, $\omega_z = 167$ kHz; ω_z is correspondingly high by about 5%. However, for m/z 1340, ω_z is 16.7 kHz.

(d) Mass range

The upper limit of the mass range is given by the mass/charge ratio having a q_z value of, let us say, exactly 0.900 when the maximum r.f. amplitude is applied to the ring electrode. From Eqn (24) it is seen that $mq_z/V =$ constant; this constant can be evaluated from the above expression for q_z as 0.0797. With $q_z = 0.900$ and $V = 7340$ $V_{(0-p)}$, the mass range for singly charged ions is found to be 650 Da.

(e) Mass range extension

With $V = 7340$ $V_{(0-p)}$ and ion ejection brought about by axial modulation at, say, $q_z = 0.900$, the upper mass limit of the ion trap is 650 Da; that is, for m/z 650, $q_z = 0.900$. However, under these trapping conditions, ions of m/z 1300 remain stored in the ion trap and have a q_z value of 0.450. If resonant excitation had been carried out at $q_z = 0.45$ with excitation at 167 kHz (see above), ions of m/z 1300 would be on the point of ejection at the maximum r.f. amplitude and the mass range of the ion trap for singly charged ions would have been doubled to 1300 Da. Similarly, with resonant excitation at $q_z = 0.045$, the mass range would be extended to 13 000 Da. This method has been applied[17] with great success, using axial modulation at low q_z and a slightly lower drive frequency Ω, such that the mass/charge range was extended to 72 000 Da per charge.

(f) Mass resolution

The normal mass scan rate of Finnigan and Varian ion traps prior to 1995 was 5555 Da s^{-1} and, over the normal mass range of 10–650 Da, the peak width was maintained at $\sim$0.5 Da. Mass resolution is defined as the ratio of mass to peak width, hence mass resolution increases with mass, but this statement is somewhat misleading as can be seen from the following example; mass resolution for m/z 65 is $\sim$130 while that for m/z 650 is 1300. The real performance of the instrument is gauged from the width of the ion signal produced upon ion ejection. Upon reducing the scan rate, it was found[18] that the peak width was reduced so that, for a given mass, mass resolution was increased. Although in research instruments peak widths of less than 3 mDa have been observed, the narrowest peak widths in com-

mercial instruments are ~0.2 Da, so that, for m/z 2000, a mass resolution approaching 10 000 is achieved.

(g) $\bar{D}_z$

The essential importance of the potential well depth is that it determines the amount of kinetic energy which an ion may acquire through resonant excitation prior to being ejected from the ion trap. The magnitude of the potential well in the z-direction may be estimated from the approximation that $\bar{D}_z \approx q_z V/8$; thus, for our example of m/z 134 at $q_z = 0.450$,

$$\bar{D}_z \approx 0.45 \times 757\ V/8 = 43\ \text{V}$$

OPERATION OF THE ION TRAP AS A MASS SPECTROMETER

We shall use dioxin (2,3,7,8-tetrachlorodibenzo-*p*-dioxin) for the purpose of illustrating the use of the ion trap as a mass spectrometer; dioxin is an excellent example of the application of ion trap mass spectrometry to analytical chemistry. Compounds such as dioxin are often determined in complex mixtures where they may be present in trace amounts and, under such circumstances, gas chromatography is a common method for sample introduction; in this example, we shall use ~400 pg of dioxin dissolved in 2 μL of *n*-nonane. The pressure of helium in the ion trap is set at about 10^{-3} Torr in order to provide adequate cooling of ions formed; while helium can be used directly from a cylinder, the helium carrier gas flowing through a chromatograph normally provides an adequate background pressure in the ion trap.

Dioxin molecules elute directly into the ion trap where they are bombarded with electrons of 50–80 eV emitted from a heated filament and gated into the ion trap, as shown in Fig. 10(a). The duration of ionization is sufficient to produce a pre-selected number of ions in a process known as automatic gain control (AGC); the ion number formed during an ionization burst of 200 μs is used to scale the ionization time in order to produce the required number of ions. The ions thus formed come immediately under the influence of the trapping potential within the ion trap. During ionization, the ring electrode is driven at an initial r.f. voltage V_0 and a fixed frequency ($f \approx 1$ MHz in many instruments), so that all ions in a given range of mass/charge ratio are trapped within the imposed quadrupole field. The value of the initial r.f. voltage V_0 imposes an LMCO, usually in the range m/z 20–50, so that ions of lower mass/charge ratio are not stored. No d.c. potential is applied between the ring and end-cap electrodes ($U = 0$) so that the confining field is purely oscillatory. During and after ionization, ions follow Lissajous-type trajectories and are subjected simultaneously to about 20 000 collisions per second with helium; those ions which are not lost from the ion trap become focused near the trap centre. In Fig. 10(b), the r.f. amplitude is ramped over the period 30–85 ms, during which mass-selective ion ejection and mass analysis occur.

Each ion species confined within the ion trap is associated with a q_z value which is calculated according to Eqn (24) and which lies on the q_z-axis on the stability diagram; ions of relatively high mass/charge ratio have q_z values near the origin while ions of lower mass/charge ratios have q_z values which extend towards the $\beta_z = 1$ stability boundary, as shown diagrammatically using stick-people of various sizes in Fig. 11(a). At the

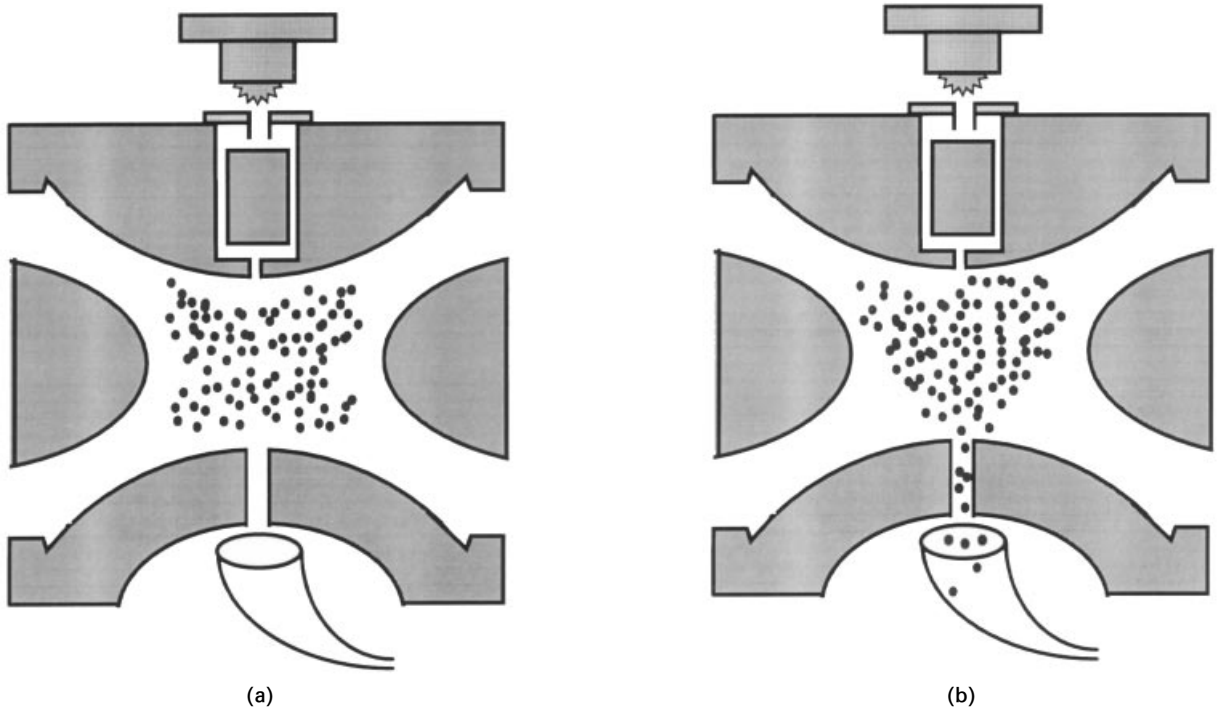

(a) (b)

Figure 10. An overview of MS-in-time. Step 1: a trapping r.f. amplitude is applied for 0–30 ms during which ions are formed from sample molecules and stored. Step 2: an r.f. amplitude is ramped over the period 30–85 ms during which mass-selective ion ejection and mass analysis occurs.

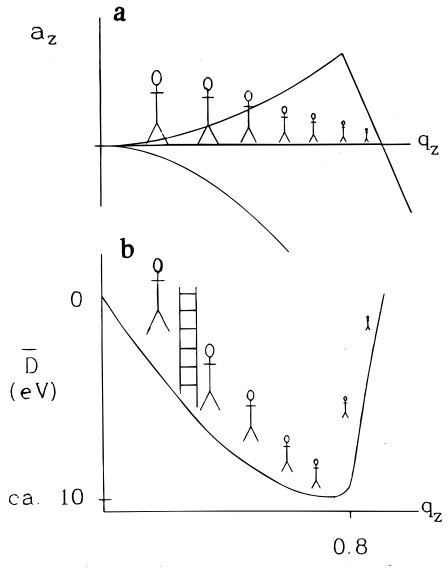

Figure 11. (a) Schematic representation of working points (that is, coordinates in a_z, q_z space) in the stability diagram for several species of ions stored concurrently. The arrangement of working points with respect to mass/charge ratio is depicted by figures which differ in size. (b) Ions are shown residing near the bottom of their respective axial potential wells of depth $\bar{D}_z$; the ladder represents the opportunity for resonant ejection of an ion species.

intersection of the $\beta_z = 1$ stability boundary and the q_z-axis, where $q_z = 0.908$ (see Fig. 7), the trajectories of trapped ions become unstable axially such that ions of mass/charge ratio less than the LMCO are not stored.

Once the ion cloud within the ion trap has been focused collisionally to the centre of the trap over a period of some 1–30 ms, the amplitude of the r.f. potential is ramped. The ramping of the r.f. potential amplitude, which is described as an *analytical ramp* or *analytical scan*, causes the q_z values of all ion species to increase throughout the ramp. As the q_z value for each ion species reaches a value of 0.908, the ions are ejected axially through the end-cap electrodes. This method of ion ejection, which can occur only at a boundary of the stability diagram and is referred to as *mass-selective axial instability*, has been supplanted by the use of axial modulation. Originally, axial modulation was the name given to resonant ejection of ions at a frequency of 485 kHz and at a q_z value only slightly less than 0.908.

When the r.f. amplitude is ramped, ions come into resonance at 485 kHz as their q_z values approach 0.908; in this manner, ions are ejected axially in order of increasing mass/charge ratio. As ions are focused near the centre of the ion trap rather in the fashion of an onion, resonance ejection has the effect of removing the ions of low mass/charge ratio residing in the innermost layer of the onion from the influence of space charge perturbations induced by other ion species so that ions are ejected free of space charge and with enhanced mass resolution. An additional advantage of resonant ejection is that it can be carried out at any frequency. Resonant ejection is depicted pictorially in Fig. 11(b) where ions are shown residing near the bottom of their respective axial potential wells of depth $\bar{D}_z$; the ladder represents the opportunity for resonant ejection of an ion species at any frequency. For axial modulation, the ladder is positioned at a q_z value just slightly less than 0.908. Resonantly ejected ions pass through holes in the end-cap electrodes so that only half of them impinge upon an electron multiplier located behind one of the end-cap electrodes; ion signals are created which produce a mass spectrum in order of increasing mass/charge ratio. The quadrupole ion trap functions as a mass spectrometer when operated in this manner.

A mass spectrum is obtained by running the scan function (see below) a number of times specified by the number of microscans; the signals which compose the mass spectrum are the result of averaging those obtained from each microscan. In the following example of obtaining a mass spectrum, one mass spectral file was generated each second. A mass spectrum of 2,3,7,8-

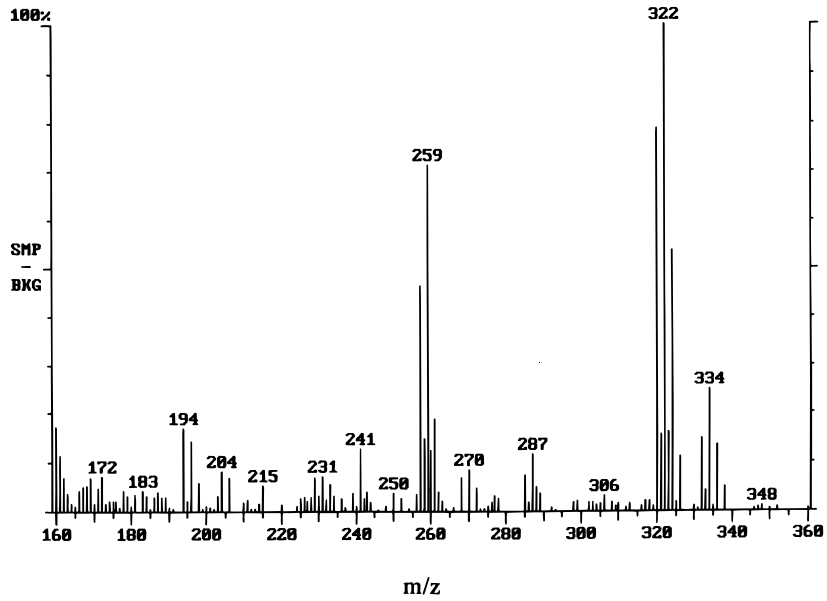

Figure 12. Mass spectrum of 2,3,7,8-tetrachlorodibenzo-*p*-dioxin. The $[M + 2]^{+\cdot}$ ion of the molecular cluster is shown at *m/z* 322 while that of a trace of $[^{13}C_{12}]$-2,3,7,8-tetrachlorodibenzo-*p*-dioxin is shown at *m/z* 334; the primary fragmentation process is the loss of COCl$^{\cdot}$ giving rise to *m/z* 259 and 270, respectively.

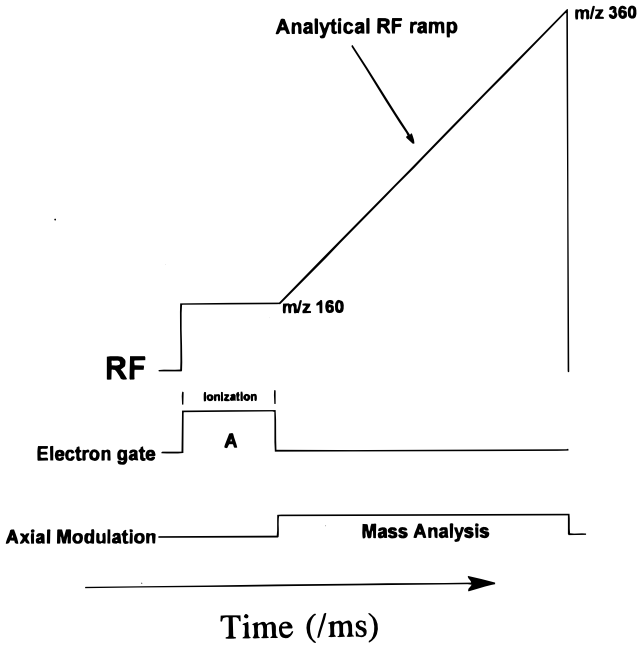

Figure 13. Scan function for obtaining an EI mass spectrum. The scan function shows the ionization period, A, followed immediately by the analytical ramp with concurrent axial modulation. Note that the pre-scan for the automatic gain control algorithm is not shown.

tetrachlorodibenzo-*p*-dioxin obtained in this manner is shown in Fig. 12. $M^{+\cdot}$ is of *m/z* 320 and the $[M + 2]^{+\cdot}$ ion of the molecular cluster which is shown at *m/z* 322 corresponds to the inclusion of one ^{37}Cl atom; the ion of *m/z* 259 is a primary fragment ion and is due to the loss of $COCl^{\cdot}$ from $[M + 2]^{+\cdot}$ and of $CO^{37}Cl^{\cdot}$ from $[M + 4]^{+\cdot}$. The peak at *m/z* 334 is $[M + 2]^{+\cdot}$ from a relatively small amount of ^{13}C-labelled $[^{13}C_{12}]$-2,3,7,8-tetrachlorodibenzo-*p*-dioxin, $M^{+\cdot}$ of *m/z* 332, added to the sample injected.

SCAN FUNCTION

The sequence of events described above can be expressed succinctly in a scan function which shows the temporal variation of all of the potentials applied to the ion trap electrodes. A scan function is a visual representation of the sequence program segments in the software which controls ion trap operation. The scan function for the mass spectrometric operation of the ion trap described above is shown in Fig. 13.

COLLISION-INDUCED DISSOCIATION

Collision-induced dissociation (CID) of an isolated ion species in a quadrupole ion trap has become a powerful technique for both the determination of ion structures and the analytical determination of, for example, compounds of environmental interest such as dioxin. Before we explore each of these uses, let us consider the CID process, how ion dissociation is effected, the efficiency of the process and the duration.

While CID is effected by resonant excitation of a selected ion species in the ion trap, the process is made more complex since the frequencies of ion motion change slightly as an ion moves away from the ion trap centre and are also dependent on space charge, that is, on the number and nature of other ions present in the ion trap. The variation in axial frequency with axial excursion, which is shown in Fig. 14 as obtained from analysis of simulated ion trajectories, arises from the superimposition of higher-order field components as a result of the axial 'stretching' of the ion trap.[19] The secular frequency variation necessitates the development of strategies for optimizing CID, particularly when the duration of irradiation must be minimized as in GC/MS analytical applications; these strategies include secular frequency modulation, single-frequency

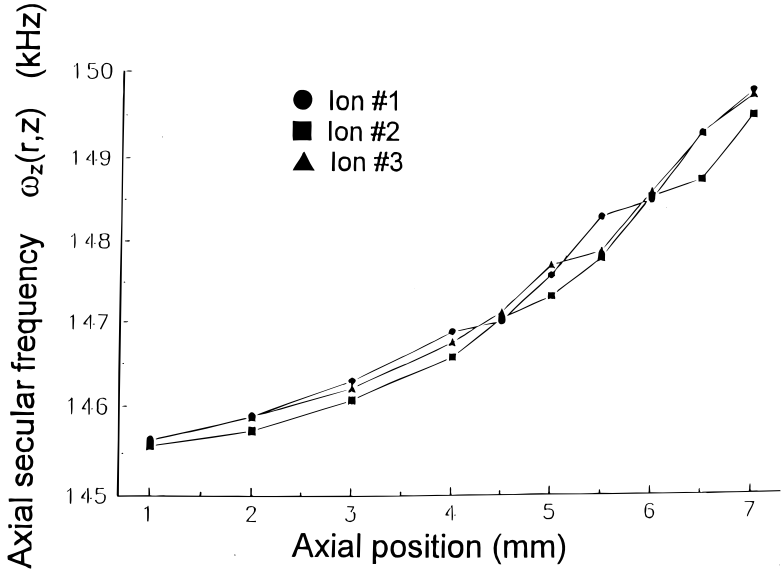

Figure 14. Variation of ion axial secular frequency as a function of the axial excursion from the centre of the ion trap. Ion trajectories were calculated for three *m/z* 134 ions, 1 (●), 2 (■) and 3 (▲), with $q_z = 0.4$ and subjected to resonant excitation. While the three ions differed in their initial position and velocity, all were close to the centre of the ion trap and had been cooled collisionally. When specific axial excursions had been reached, excitation was arrested and the trajectory subjected to frequency analysis.

irradiation with r.f. modulation and multiple-frequency irradiation.

Under the influence of the applied resonant excitation voltage, ions are moved away from the centre to a region of higher potential whereupon they are accelerated (under the influence of the higher potential rather than the resonant excitation voltage alone) so that their kinetic energies are increased. Subsequent collisions with buffer gas atoms lead to enhancement of ion internal energy. Ions undergo rapid changes in kinetic energy on the microsecond time-scale whereas changes in internal energy occur more slowly on the millisecond time-scale. In analytical applications, the objective is usually to dissociate all of the isolated ions and to maximize the trapping of fragment ions produced; the achievement of this objective requires a balancing of ion kinetic energy uptake so that ion internal energy may be accumulated incrementally and rapidly but ejection of both isolated ions and fragment ions is prevented. Incremental loss of internal energy in collisions can occur with both buffer gas atoms and sample molecules while total loss of internal energy can occur upon charge exchange with sample molecules; yet these loss mechanisms merely slow down the overall accumulation of internal energy as there is no net loss of charge involved.

The role played by time is enormously important in CID. The total time during which ions are subjected to collisions and the total time during which ions are subjected to irradiation can be used as variable parameters to direct dissociation into a chosen fragmentation pathway. While the mode of irradiation is influential also in directing fragmentation, alternating periods of irradiation (with collisions) and collisional cooling can affect significantly the fragment ion abundances. During an irradiation period, the time-averaged ion kinetic energies increase along with internal energy: during a subsequent collisional cooling period in which the excitation voltage is removed, ion kinetic energies are quenched more readily than are ion internal energies. Thus ions become kinetically relaxed during a cooling period and sample once more the lower reaches of the trapping potential well yet the internal energies gained are virtually unimpaired. The internally excited ions, kinetically cool and focused near the centre of the ion trap, can be excited further during the next irradiation period. In this manner, several electronvolts of internal energy can be deposited in ions so as to access fragmentation pathways of high activation energy.

TANDEM MASS SPECTROMETRY

Tandem (Latin: *at length*) mass spectrometry (MS/MS) is the practice of carrying out one mass-selective operation after another, much as one rider is seated after the other on a tandem bicycle. The objective of the first mass-selective operation is to isolate an ion species designated as the *parent* ion, while that of the second operation is to determine the mass/charge ratios of the fragment, or *product*, ions formed by CID of the parent ions. MS/MS can be effected in space, by placing one mass spectrometer after another, or by carrying out successive mass-selective operations in time in a quadrupole ion trap. The ion trap offers two principal advantages when used in the MS/MS mode. First, the ion trap operates in a pulsed mode, in contrast to sector and triple-stage quadrupole instruments which operate in a continuous mode, so that it can accumulate ions mass selectively over time. In this way, a target ion number can be selected so as to ensure constant signal-to-noise ratio over a wide range of eluent concentrations. A disadvantage of ion accumulation is that the resultant product ion signal intensity can correspond to integration of eluent concentration over $\sim$25 ms. Second, CID in the ion trap is wrought by several hundred collisions of mass-selected ions with helium buffer gas atoms. Under these conditions, the energy transferred in a single collision is seldom greater than a few vibrational quanta such that the dissociation reaction channels of lowest energy of activation are accessed almost exclusively; this behaviour is highly advantageous in analytical chemistry in that the total charge is conserved within a single fragment ion species. However, alternating periods of excitation and collisional cooling can be used to access dissociation reaction channels of higher energy of activation. Furthermore, it is possible to dissociate completely the accumulated mass-selected ions and to confine within the ion trap fragment ions arising from $\sim$90% of the accumulated mass-selected ions in favourable cases.

To achieve CID with such high efficiency (defined as 100 times the ratio of the sum of product ion signal intensities to that the parent ion) when the ion trap is interfaced with a gas chromatograph, it is imperative that the resonant excitation conditions be optimized with respect to the duration of the CID episode. Here, we use multifrequency irradiation (MFI) as it has been shown to be an effective method for CID because it exhibits high efficiency and requires a relatively short period of irradiation, $\sim$10 ms.

$(MS)^2$

Here, MS/MS is illustrated using an extension of the dioxin example used in the above discussion. This application,[20] while not illustrating the ultimate limit of sensitivity of the ion trap of some hundreds of femtograms of dioxin, does illustrate the high sensitivity of the ion trap for the determination of co-eluting dioxin congeners. Polychlorodibenzo-*p*-dioxins (PCDDs) and polychlorodibenzofurans (PCDFs) are persistent chlorinated organic compounds in the environment; most of these chloro congeners are obtained from municipal and industrial waste incinerators, automobile exhaust and the manufacture of chlorophenol products. The compounds having the highest toxicities have been identified as those congeners having 2,3,7,8-tetrachloro substitution. When gas chromatography is interfaced with mass spectrometry, individual chloro congeners can be detected at the hundreds of femtograms level. The high specificity or informing power obtainable with GC/MS/MS is achieved by observation of specific fragment ion signals, such as $[M - COCl^{\cdot}]^+$, from an isolated ion species $M^{+\cdot}$ formed from M which elutes within a specified retention-time window. The essential

stages of MS/MS are portrayed in the scan function for dioxin shown in Fig. 15. It is instructive to examine this scan function in advance of the following explanation of ionization, ion isolation, cooling period, CID and the analytical ramp over a selected mass range so as to detect product ions.

We shall examine the MS/MS of $[M]^{+\cdot}$ and $[M + 2]^{+\cdot}$ for T_4CDF, T_4CDD and their internal (labelled) standards following elution from a GC column, where $[M + 2]^{+\cdot}$ is a molecular ion containing a single ^{37}Cl atom.

Scan functions

The scan function employed for the MS/MS determination of T_4CDDs is shown in Fig. 15. The r.f. voltage is applied to the ring electrode with a drive frequency f of 1.05 MHz. The LMCO value, as determined by the amplitude of the r.f. potential, was set at m/z 160 during the ionization period (A) for all the scan functions so that the q_z value for $M^{+\cdot}$ (m/z 320) was 0.45. While the same scan function can be used for all T_4CDDs as they do not co-elute, different scan functions must be used in sequence for the determination of a specific T_4CDD and its co-eluting labelled isotopomer.

A total ion number target of 35 000 counts was set for the AGC algorithm; with a filament emission current of 50 μA, the maximum ionization time employed was 20 ms. The supplementary alternating voltages applied to the end-cap electrodes in dipolar fashion are referred to as waveforms; these waveforms are employed for ion isolation, ion excitation and axial modulation. A pre-isolation waveform was imposed during ionization (A) and prolonged after the cessation of ionization during period B. The pre-isolation waveform consisted of multiple frequencies covering the range 3.7–513.5 kHz with a 1 kHz notch corresponding to the secular frequency of the molecular ions to be isolated. For the example of a T_4CDD scan function shown in Fig. 15, the notch is centered at 174.5 kHz in order to isolate both m/z 320 and 322, $[M]^{+\cdot}$ and $[M + 2]^{+\cdot}$, respectively, having q_z values of 0.454 and 0.451, respectively. The amplitude of the pre-isolation waveform was 20 $V_{(0-p)}$ for all scan functions; the function of the pre-isolation waveform was to eject all ions except the selected ones. Fine isolation was achieved by ramping the r.f. amplitude until the LCMO was just less than m/z 320 at which point ions of lower mass/charge ratios were ejected; ion ejection was facilitated by concurrent application of axial modulation with an amplitude of 3 $V_{(0-p)}$. The r.f. amplitude was modulated moderately over a small amplitude range in order to avoid ejection of the selected ions. The ejection of ions with $m/z > 322$ (C) was achieved by applying a broadband waveform having an amplitude of 30 $V_{(0-p)}$ and lasting for 5 ms.

Once isolation of the selected ion species [m/z 320 and 322 for T_4CDD as illustrated in Fig. 16(a)] was completed, the r.f. amplitude was reduced to obtain a q_z value of 0.4 for m/z 322; for T_4CDD, a q_z value of 0.4 for m/z 322 corresponds to an LCMO value of m/z 142. The bandwidth of the waveform employed to carry out CID using multifrequency irradiation (MFI) was composed of 13 frequency components spaced at intervals of 0.5 kHz so as to cover a 6 kHz band of frequencies. The total bandwidth is almost double the required bandwidth since the Toolkit software locks the centre of the MFI band to the axial secular frequency of the previously selected ion species; only the width of the MFI band can be varied. The MFI waveform amplitudes were 2.55 $V_{(0-p)}$ for T_4CDF and 2.45 $V_{(0-p)}$ for T_4CDD. The voltage amplitude of each component of the MFI waveform is equal to the amplitude of the waveform divided by the number of frequency components.

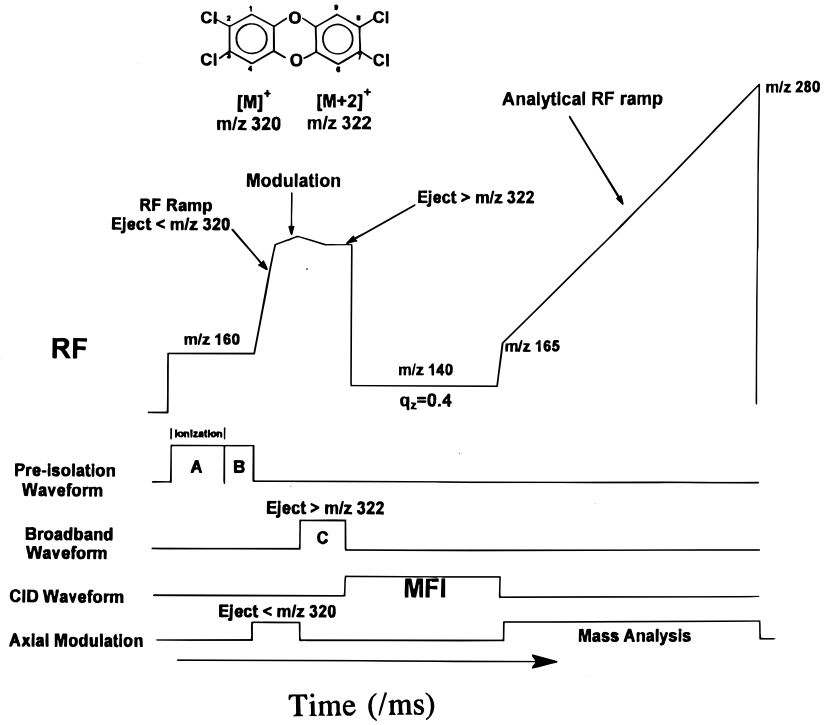

Figure 15. Scan function for MS/MS of dioxin (T_4CDD); the pre-scan for AGC is not shown.

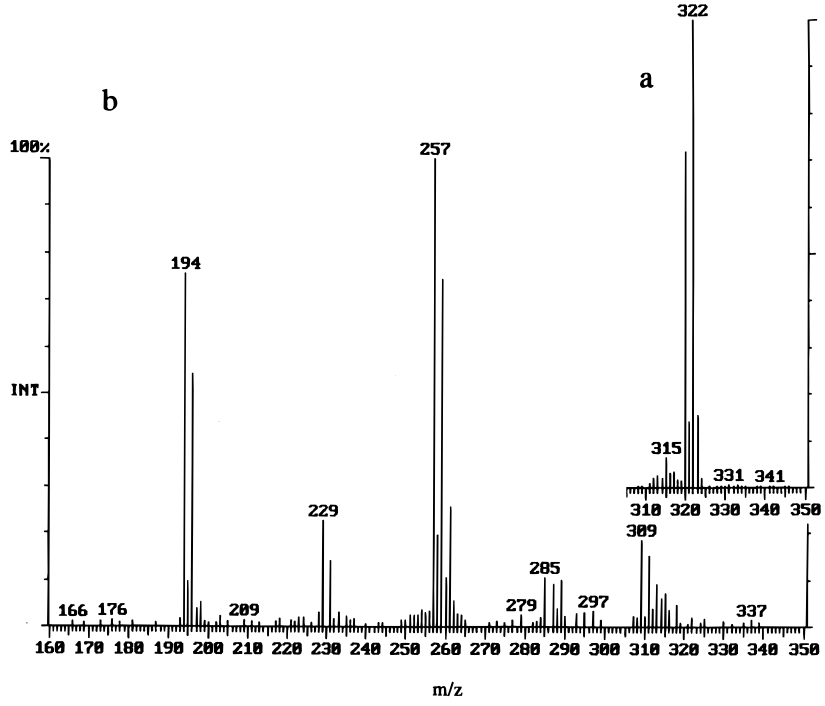

Figure 16. Mass spectra of T_4CDD: (a) mass spectrum showing the isolated $[M]^{+\cdot}$ and $[M+2]^{+\cdot}$ ions of the molecular ion cluster; (b) product ion mass spectrum obtained by CID of the two isolated ion species shown in (a). Note the complete disappearance of the isolated molecular ions.

Following CID by MFI for 10 ms, the analytical mass range of 165–350 Da was scanned for product ions from T_4CDF and T_4CDD so as to monitor all major product ions save that resulting from chlorine atom loss. A mass spectrum of the product ions from dioxin is shown in Fig. 16(b): *m/z* 257 and 194 are due to the losses of $COCl^{\cdot}$ or $2COCl^{\cdot}$, respectively, from $M^{+\cdot}$ (*m/z* 320). The analytical ramp was scanned at 5555 Da s^{-1}; axial modulation was carried out with an amplitude of 3 $V_{(0-p)}$ and at a frequency of 485 kHz. The electron multiplier was biased at a voltage of ~1800 V to provide an ion signal gain of 10^5.

Each scan function used had a duration of ~125 ms such that each acquisition point or mass spectral file was generated from four microscans; thus two mass spectra were accumulated each second. It should be noted that when a small mass range is monitored during the analytical r.f. ramp, say for two fragment ions only, the duration of the scan function can be reduced to only 50 ms such that the number of mass spectral files can be increased to five per second, each based on four microscans. The mass spectra obtained from the application of each scan function within an ion preparation file were merged together to form a single merged mass spectra. The significance of this merging procedure is described below.

MS/MS DETERMINATION OF ELUTING AND CO-ELUTING COMPOUNDS

The total ion chromatogram shown in Fig. 17 was obtained by GC/MS/MS of 1 μL of solution containing 200 pg of each of a T_4CDF, a $[^{13}C_{12}]T_4CDF$, a T_4CDD and a $[^{37}Cl_4]T_4CDD$ and 100 pg of each of two $[^{13}C_{12}]T_4CDDs$. The peak indicated with an asterisk in Fig. 17 is an impurity present in the sample. This chromatogram is described more properly as a merged total ion chromatogram since it is a display of the total ion count of each merged mass spectrum obtained as described above.

Let us consider the first three peaks of interest which were observed in this merged total ion chromatogram, that is, those peaks labelled 1, 2 and 3. Peak 1 is due to a T_4CDF and its co-eluting $^{13}C_{12}$-labelled isotopomer (a component of the solution injected); peak 2 is due solely to a $[^{13}C_{12}]T_4CDD$ and peak 3 is a composite peak of a native T_4CDD and its $^{13}C_{12}$- and $^{37}Cl_4$-labelled isotopomers.

For the T_4CDF of molecular mass is 304, the molecular ion $M^{+\cdot}$ of *m/z* 304 and the $[M+2]^{+\cdot}$ of *m/z* 306 were isolated simultaneously then dissociated collisionally using MFI in accordance with a specific scan function. The signal intensities of the fragment ions arising from the loss of $COCl^{\cdot}$ or $CO^{37}Cl^{\cdot}$ to yield *m/z* 241 and 243 were recorded and summed as shown in Fig. 18. For MS/MS of the co-eluting $[^{13}C_{12}]T_4CDF$, the second scan function comes into play for the ionization and simultaneous isolation of both $M^{+\cdot}$ of *m/z* 316 and $[M+2]^{+\cdot}$ of *m/z* 318; the isolated ion species were then subjected to CID with MFI. The signal intensities of the fragment ions arising from the loss of $COCl^{\cdot}$ or $CO^{37}Cl^{\cdot}$ to yield *m/z* 252 and 254 were recorded and summed as shown in Fig. 18. Throughout the period when the native and labelled T_4CDFs are co-eluting, the first two scan functions are used alternately.

Now let us consider peak 2 in Fig. 17. A third scan function is required for the MS/MS determination of the labelled $[^{13}C_{12}]T_4CDD$ to control the ionization, isolation and CID of both the molecular ion $M^{+\cdot}$ of *m/z* 332 and the $[M+2]^{+\cdot}$ of *m/z* 334. The signal intensities

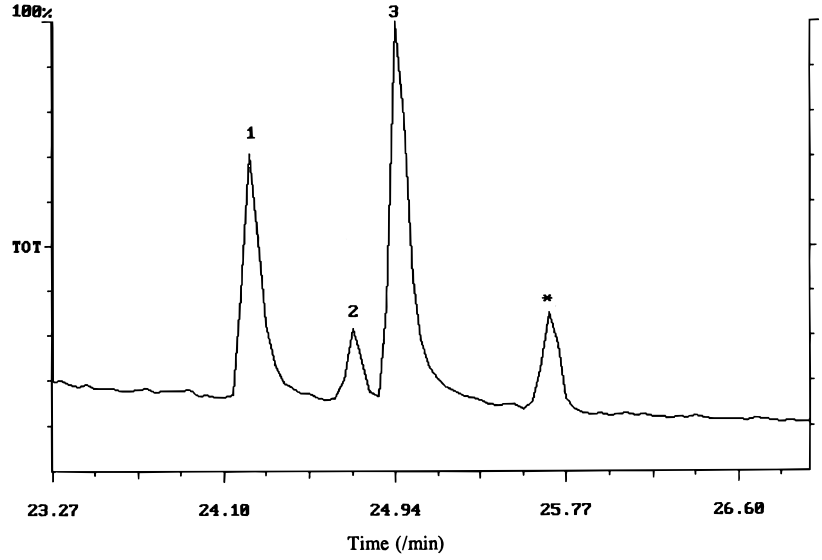

Figure 17. A merged total ion chromatogram of six dioxins and furans and their labelled isotopomers. Each point expresses the sum of all of the relevant fragment ion peaks.

of the fragment ions arising from the loss of $COCl^{\cdot}$ or $CO^{37}Cl^{\cdot}$ to yield m/z 268 and 270 were summed and recorded in Fig. 18.

Peak 3 in Fig. 17 is composed of the fragment ion counts from three compounds. The scan function used in peak 2 was used again for the MS/MS determination of a T_4CDD together with two additional scan functions for the co-eluting $[^{13}C_{12}]$ and $[^{37}Cl_4]T_4CDD$ isotopomers. For the T_4CDD of molecular mass 320, the molecular ion $M^{+\cdot}$ of m/z 320 and the $[M + 2]^{+\cdot}$ of m/z 322 were isolated simultaneously then dissociated as before and the signal intensities of the fragment ions of m/z 257 and 259, as shown in Fig. 16, were summed and recorded in Fig. 18. From the MS/MS of the $[^{13}C_{12}]T_4CDD$, the signal intensities of the fragment ions of m/z 268 and 270 were summed and recorded in Fig. 18. For the MS/MS of the $[^{37}Cl_4]T_4CDD$ of molecular mass 328, the molecular ion $M^{+\cdot}$ of m/z 328 was isolated then dissociated as before and the signal intensity of the fragment ions arising from the loss of $CO^{37}Cl^{\cdot}$ to yield m/z 263 was recorded in Fig. 18.

The signal areas of each of the six separated compounds are shown in Fig. 18 as selected ion chromatograms; the signal intensities of fragment ions due to loss of $COCl^{\cdot}$ or $CO^{37}Cl^{\cdot}$ only are plotted here. In order to perform MS/MS on the total of six different tetrachlorinated dioxins and furans which constituted the first three peaks of Fig. 17, a total of five different scan functions was required. In this example, the enormous power of MS/MS is evident in the determination of three co-eluting compounds.

In the above discussion, only a single fragmentation channel was considered, that of the loss of $COCl^{\cdot}$ or $CO^{37}Cl^{\cdot}$. While $COCl^{\cdot}$ loss is the major fragmentation channel, it is not the sole loss channel. For the dioxins, minor losses of $Cl^{\cdot}$ and $2COCl^{\cdot}$ are observed whereas for the furans, minor losses of $Cl^{\cdot}$, $COCl_2$ and $COCl_3^{\cdot}$ are observed. The duration of the analytical r.f. ramp

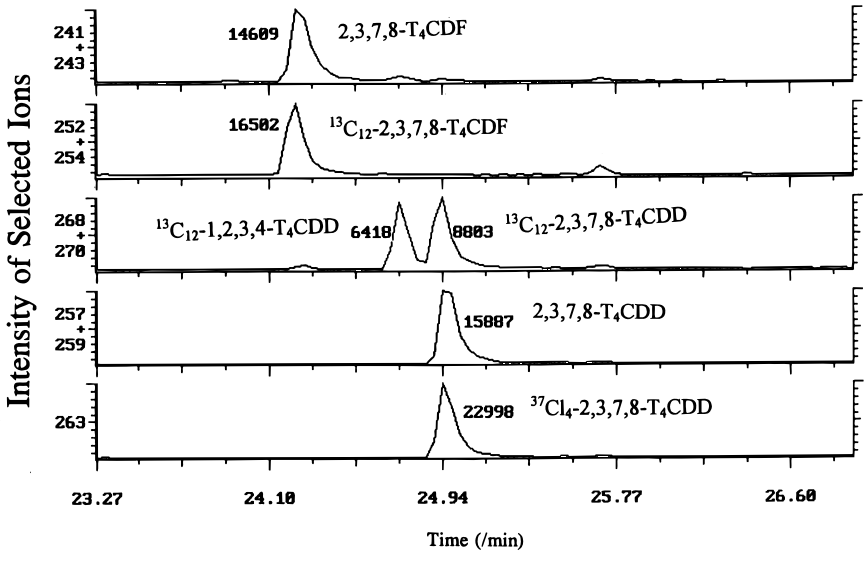

Figure 18. Selected ion chromatogram showing that the signal area of each of six compounds can be determined using GC/MS/MS.

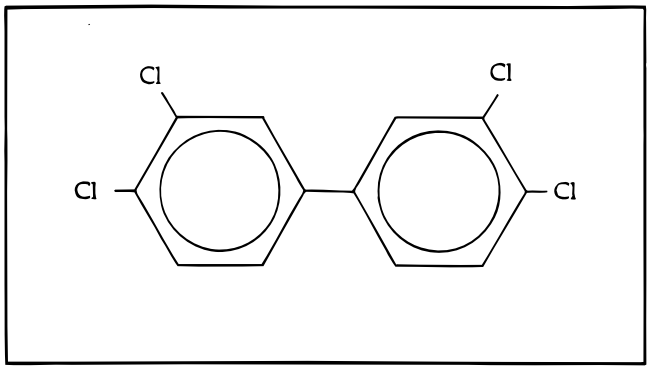

Congener 77

3, 3', 4, 4' - tetrachlorobiphenyl

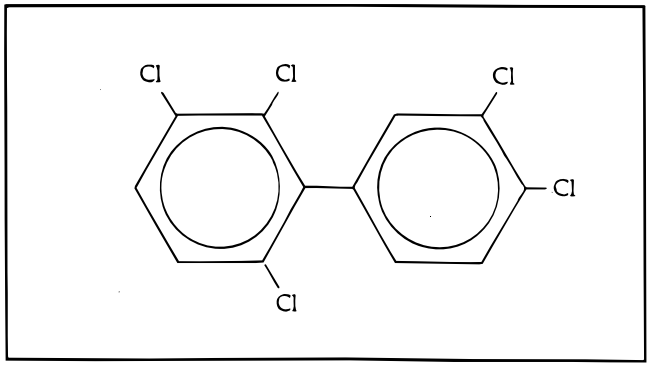

Congener 110

2, 3, 3', 4', 6 - pentachlorobiphenyl

Scheme 1. PCB congeners 77 and 110.

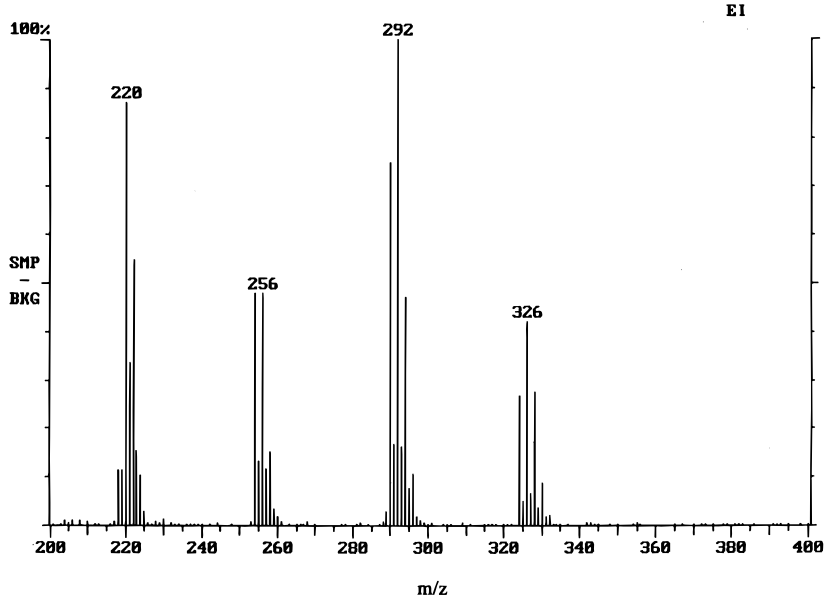

Figure 19. EI mass spectrum averaged over the GC composite peak of the co-eluting polychlorinated congeners 77 and 110.

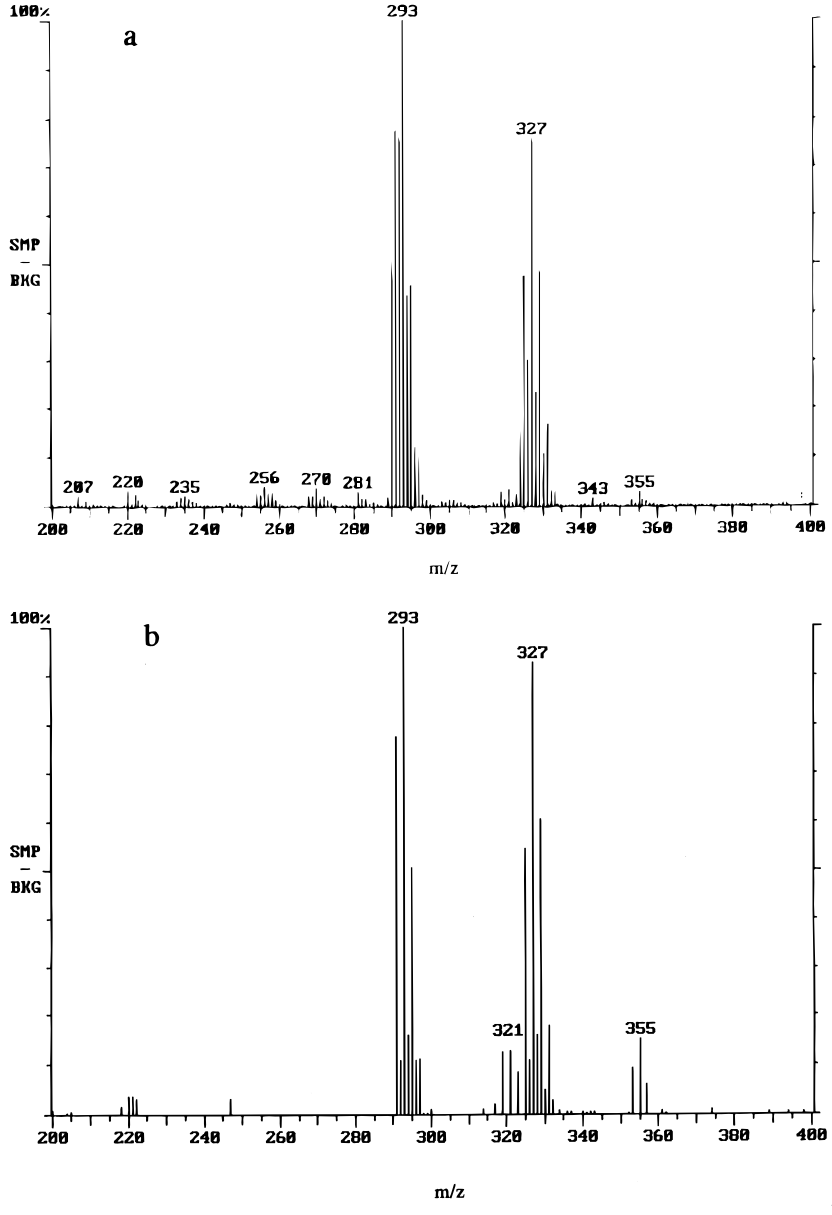

Figure 20. (a) Chemical ionization mass spectrum averaged over the GC composite peak of the co-eluting polychlorinated biphenyl congeners 77 and 110; methane CI gas at a pressure and reaction time such that the ratio of signal intensities of *m/z* 29 and 17 was 1 : 1. (b) Selected reagent ion chemical ionization mass spectrum averaged over the GC composite peak of the co-eluting polychlorinated biphenyl congeners 77 and 110 using *m/z* 29 from methane.

was reduced by choosing a small mass range that excluded the fragment ions of low abundance.

(MS)^n

The above sequence of ion isolation and CID can be repeated many times in a process known as (MS)^n. While this process is not illustrated here, multiple stages of mass-selective operation are used frequently for ion structure determination where the quadrupole ion trap is used in combination with external ionization sources, such as electrospray ionization. Here, multiply charged molecules having masses in the thousands of dalton can be stored in an ion trap and subjected to (MS)^n so as to follow the stepwise ion dissociation for the elucidation of ion structure.

CHEMICAL IONIZATION AND ION–MOLECULE REACTIONS

In the quadrupole ion trap, several types of reactions can and do occur simultaneously and spontaneously once electron ionization of a compound has occurred. Ion–molecule reactions involving charge transfer, proton transfer and clustering occur sequentially in a type of thermodynamic 'waterfall' which results in the

formation of stable even-electron ions of greater mass/charge ratio than that of the molecular ion. Proton transfer chemical ionization (CI) involves the transfer to a neutral species of a proton from an ion which has been formed in an ion–molecule reaction. Parenthetically, CI can be effected by the transfer of other even-electron charged particles.

Let us consider the CI of the co-eluting polychlorinated biphenyl (PCB) congeners 77 and 110 shown in Scheme 1.[21] Congener 77, which is highly toxic, is a non-*ortho* compound in that the molecule is not chlorine substituted in the *ortho* positions vicinal to the phenyl–phenyl bond. On the other hand, congener 110 is a mono-*ortho* compound and is much less toxic. Since the concentration of toxic congener 77 in environmental samples is often $<1\%$ of that of congener 110, quantitative analysis of congener 77 is a challenge.

The EI mass spectrum, averaged over the GC composite peak of the co-eluting congeners 77 and 110, is shown in Fig. 19. The base peak group in the mass spectrum is the molecular ion cluster of the tetrachloro congener 77, where m/z 292 is $[M_{77} + 2]^{+\cdot}$; this peak is superimposed on the fragment ion cluster due to the loss of one chlorine atom from pentachloro congener 110 $[M_{110} + 2]^{+\cdot}$, m/z 326, where m/z 291 is $[M_{110} + 2 - Cl]^{+\cdot}$. The peak at m/z 220 is due to loss of $2Cl^{\cdot}$ from $[M_{77} + 2]^{+\cdot}$ and $3Cl^{\cdot}$ from $[M_{110} + 2]^{+\cdot}$, while the peak at m/z 256 is due principally to the loss of $2Cl^{\cdot}$ from $[M_{110} + 2]^{+\cdot}$. It is not possible to determine quantitatively the relative contributions of the two congeners to this mass spectrum. Now let us examine the CI of these congeners using methane as the CI reagent.

The ionization of methane yields the molecular ion which reacts with methane to form CH_5^+:

$$CH_4^{+\cdot} + CH_4 \rightarrow CH_5^+ + CH_3^{\cdot} \qquad (29)$$

and the CH_3^+ ion which reacts with methane to form $C_2H_5^+$:

$$CH_3^+ + CH_4 \rightarrow C_2H_5^+ + H_2 \qquad (30)$$

In practice, an LMCO of $m/z \approx 12$ is established by the r.f. amplitude, then methane is introduced briefly into the ion trap and ionized simultaneously with the congeners. Owing to the preponderance of methane, CH_5^+ and $C_2H_5^+$ are formed rapidly during a short interval inserted into the scan function for ion–molecule reactions and can be isolated; during the isolation process, primary ions of methane and the congeners together with other secondary ions from methane are ejected and surplus methane is pumped away. Proton transfer then occurs during a reaction period of ~ 10 ms.

When methane is used as a CI reagent with a reaction time such that the signal intensities of CH_5^+ and $C_2H_5^+$ are similar, CI of a mixture of congeners 77 and 110 yields a mixture of proton transfer CI (to form $[M + H]^+$) and charge transfer (to form $M^{+\cdot}$), as shown in Fig. 20(a). However, when a single reagent ion species, in this case m/z 29, is isolated for CI, proton transfer only is observed for both congeners, ($[M_{77} + 2 + H]^{+\cdot}$, m/z 293 $[M_{110} + 2 + H]^{+\cdot}$, m/z 327), as shown in Fig. 20(b). The isotopic ratios for each cluster of protonated congeners are in good agreement with those expected for pure CI: the contribution of charge exchange to the congener 77 molecular cluster is 3%. The mass spectrum is entirely free of fragment ions below $[M_{77} + H]^+$. The adduct formation channel can be suppressed by reducing reagent gas pressure.

Now that external ion sources can be used with an ion trap, CI reagent ions can be created externally and injected subsequently into the ion trap, isolated mass selectively and allowed to react therein with sample molecules.

CONCLUSIONS

Quadrupole ion trap mass spectrometry has been shown to be a versatile technique of high sensitivity and high specificity. The relatively low cost of commercial instrumentation has permitted a substantial growth in the practice of mass spectrometry and a pronounced diminution of the average cost per mass spectrum. The theory of ion trap operation differs from those of other mass spectrometers and presents an exciting challenge to the mass spectrometry community; it is hoped that this introduction to quadrupole ion trap mass spectrometry will be useful to those wishing to overcome this barrier and enable them to enjoy the delights of this nascent branch of mass spectrometry.

Acknowledgements

The author acknowledges gratefully the financial support of the Natural Sciences and Engineering Research Council of Canada, Varian Canada and the Ontario Ministry of Environment and Energy and the assistance of Dr M. Splendore.

REFERENCES

1. G. C. Stafford Jr, P. E. Kelley, J. E. P. Syka, W. E. Reynolds and J. F. J. Todd, *Int. J. Mass Spectrom. Ion Processes* **60**, 85 (1984).
2. W. Paul and H. Steinwedel, *Ger. Pat.* 944 900 (1956); *US Pat.* 2 939 952 (1960).
3. W. Paul, *Angew. Chem.* **29**, 739 (1990).
4. P. H. Dawson and N. R. Whetten, *Adv. Electr. Electron. Phys.* **27**, 59 (1969).
5. P. H. Dawson, *Quadrupole Mass Spectrometry and Its Applications*. Elsevier, Amsterdam (1976).
6. R. E. March, R. J. Hughes and J. F. J. Todd, *Quadrupole Storage Mass Spectrometry*. Wiley–Interscience, New York (1989).
7. J. F. J. Todd, *Mass Spectrom. Rev.* **10**, 3 (1991).
8. R. G. Cooks and R. E. Kaiser Jr, *Acc. Chem. Res.* **23**, 213 (1990); B. D. Nourse and R. G. Cooks, *Anal. Chim. Acta* **228**, 1 (1990).
9. G. L. Glish and S. A. McLuckey, *Int. J. Mass Spectrom. Ion Processes* **106**, 1 (1991).
10. R. E. March, *Int. J. Mass Spectrom. Ion Processes* **118/119**, 71 (1992).
11. R. E. March and J. F. J. Todd (Eds), *Practical Aspects of Ion Trap Mass Spectrometry*, Vols 1, 2 and 3. CRC Press, Boca Raton, FL (1995).
12. R. D. Knight, *Int. J. Mass Spectrom. Ion Processes* **106**, 63 (1991).

13. E. Mathieu, *J. Math. Pure Appl.* (*J. Liouville*) **13**, 137 (1868).
14. M. Nappi, C. Weil, C. D. Cleven, L. A. Horn, H. Wollnik and R. G. Cooks, *Int. J. Mass Spectrom. Ion Processes* in press.
15. H.-P. Reiser, R. E. Kaiser Jr and R. G. Cooks, *Int. J. Mass Spectrom. Ion Processes* **121**, 49 (1992).
16. M. Splendore, personal communication.
17. R. E. Kaiser Jr, R. G. Cooks, G. C. Stafford Jr, J. E. P. Syka and P. E. Hemberger, *Int. J. Mass Spectrom. Ion Processes* **106**, 79 (1991).
18. J. C. Schwartz, J. E. P. Syka and I. Jardine, *J. Am. Soc. Mass Spectrom.* **2**, 198 (1991).
19. M. Splendore, F. A. Londry, R. E. March, R. J. S. Morrison, P. Perrier and J. André, *Int. J. Mass Spectrom. Ion Processes* **156**, 11, (1996).
20. R. E. March, J. B. Plomley and M. Splendore, *Final Report on The Application of Quadrupole Ion Trap Mass Spectrometry to the Development of New Analytical Protocols for Dioxins/Furans*. Submitted to the Ontario Ministry of Environment and Energy and Varian (Canada), September 1996.
21. M. Lausevic, J. B. Plomley, X. Jiang, R. E. March and C. D. Metcalfe, *Eur. Mass Spectrom.* **1**, 149 (1995).